A CARBON NANOTUBE-BASED SENSOR FOR CO_2 MONITORING

Keat G. Ong, Padmakar D. Kichambare, and Craig A. Grimes
Center for Micro-Magnetic and Electronic Devices
Department of Electrical Engineering, 453 Anderson Hall
University of Kentucky, Lexington, KY 40506, USA.

Introduction

Carbon nanotubes, molecular-scale tubes of carbon with high mechanical strength and unique electrical properties, have seen considerable interest in recent years for applications including, to name a few, field emission devices [1], nano-electronic devices [2-5], actuators [6], and random access memory [7]. Carbon nanotubes have successfully been used as oxygen [8] and methane [9] gas sensors.

In this paper we report, apparently for the first time, application of multi-wall carbon nanotubes (MWNTs) to carbon dioxide sensing, based upon the measured changes in MWNT permittivity with CO_2 exposure. The transduction platform used in this work is a planar, inductor-capacitor resonant-circuit (LC) sensor [10,11]. A thin layer of a MWNT-SiO_2 composite is placed upon the inter-digital capacitor of the LC sensor; as the permittivity of the adjacent layer changes so does the sensor resonant frequency which is remotely monitored using a loop antenna [10]. The passive nature of the LC sensor enables long term monitoring without battery life-time issues, and the wireless nature of the platform enables monitoring of CO_2 from within sealed, opaque containers such as food or medicine packages. High levels of CO_2 within such containers are widely used as a determinant for contamination [12,13]. In addition to food quality monitoring CO_2 sensors are important for industrial process control [14], monitoring air quality [15], *etc*.

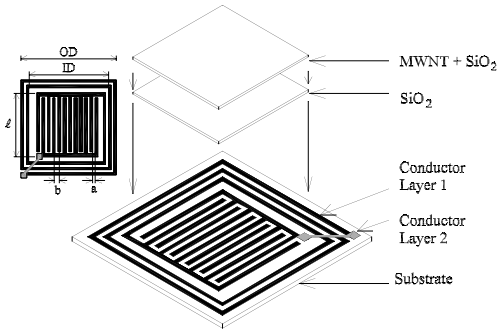

Fig. 1. Schematic drawing of CO_2 sensor. A planar inductor-interdigital capacitor pair is defined on a printed circuit board. The capacitor is first coated with a protective SiO_2 layer followed by a layer of CO_2 responsive MWNT-SiO_2 composite.

Most CO_2 sensors available on the market today operate by measuring the impedance of a capacitor coated with a CO_2-responsive material such as heteropolysiloxane [16], $BaTiO_3$ [17], $CeO/BaCO_3/CuO$ [18], Ag_2SO_4 [19], and Na_2CO_3 [19]. These CO_2 sensors offer a high degree of accuracy and reliable performance, but require hard-wire connections between the sensor head, power supply, and data processing electronics which precludes many monitoring applications.

The general sensor structure is shown in Fig. 1, and consists of a printed inductor-capacitor resonant circuit that is first coated with a protective, electrically insulating SiO_2 layer [20], followed by a second layer consisting of the CO_2 responsive MWNT-SiO_2 mixture with the SiO_2 matrix acting to physically bind the MWNTs to the sensor. As the sensor is exposed to CO_2 the relative permittivity ε_r' and the conductivity (proportional to ε_r'' [21]) of the MWNTs vary, changing the effective complex permittivity of the coating and hence the resonant frequency of the sensor. The relationship between the CO_2 adsorption and the complex permittivity is discussed within the Results & Discussion.

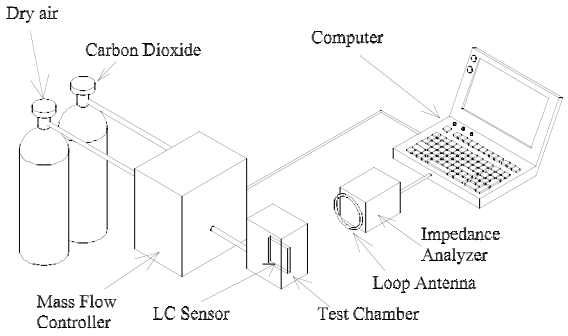

Fig. 2. Experimental setup for testing the CO_2 sensor. The sensor is placed inside a sealed Plexiglas chamber, and monitored via a loop antenna, which the impedance is measured with an impedance analyzer.

As shown in Fig. 2, the response of the CO_2 sensor is obtained by directly measuring the impedance spectrum of a sensor-monitoring loop antenna. The impedance of the loop antenna is removed from the measurement using a background subtraction, obtained by measuring the

antenna impedance without the sensor present. A typical background-subtracted impedance spectrum is shown in Fig. 3, where the resonant frequency f_0 is defined as the frequency at the real impedance (resistance) maximum, and the zero-reactance frequency f_Z is the where the imaginary impedance (reactance) goes to zero. By modeling the sensor with an RLC circuit and performing standard circuit analysis, the complex permittivity, $\varepsilon_r' - j\varepsilon_r''$, of the coating material (both the MWNT-SiO_2 and SiO_2 layers) are calculated from the measured f_0 and f_Z as [10,11]:

$$\varepsilon_r' = \frac{1}{(2\pi f_0)^2 L\kappa\varepsilon_0} - \varepsilon_s \qquad \varepsilon_r'' = \frac{\sqrt{f_0^2 - f_Z^2}}{4\pi^2 f_0^3 L\kappa\varepsilon_0} \tag{1}$$

ε_0 is the free space permittivity ($\varepsilon_0 = 8.854\times10^{-12}$ F/m), ε_σ is the relative permittivity of the electrically lossless substrate (that is $\varepsilon_s = \varepsilon_s'$), κ is the cell constant of the interdigital capacitor, and L is the inductance of the spiral inductor in Henry's. The cell constant κ and inductance L can be calculated from the sensor geometry using [22-24]:

$$\kappa = \frac{\ell(N_C - 1)K\left[(1-(a/b)^2)^{1/2}\right]}{2K[a/b]} \tag{2}$$

$$L = 1.39\times10^{-6}(OD + ID)N_L^{5/3}\log_{10}\left(4\frac{OD+ID}{OD-ID}\right) \tag{3}$$

where a, b, ℓ, OD, and ID are the dimensions of the sensor defined in Fig. 1, N_C is the number of fingers in each capacitor's electrode, N_L is the number of the inductor turns, and K is the elliptic integral of the first kind.

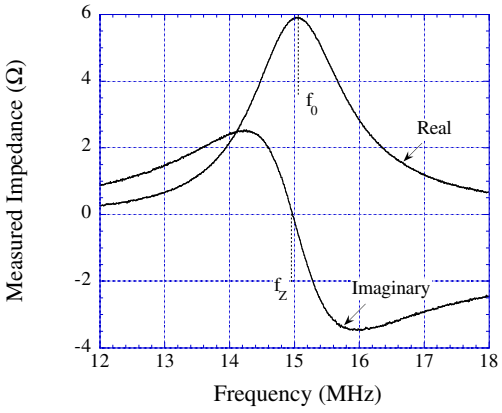

Fig. 3. An illustrative measured impedance spectrum of the sensor-perturbed antenna, after subtracting the background antenna impedance. The resonant frequency f_0 is defined as the maximal of the real portion of the impedance, and the zero-reactance frequency f_Z is the zero crossing of the imaginary portion of the impedance.

Experimental

Preparation of Carbon nanotubes

The MWNTs used in this work were prepared by pyrolysis of ferrocene and xylene under Ar/H_2 atmosphere over quartz substrates in a two-stage reactor [25]. Approximately 6.5 mol% of ferrocene was dissolved in xylene and continuously fed into a tubular quartz reactor. Ferrocene has been shown to be an excellent precursor for producing Fe catalyst particles, and xylene was selected as the hydrocarbon source. The liquid feed was passed through a capillary tube and preheated to ~175^{0}C prior to its entry into the furnace. At this temperature, the liquid exiting the capillary was immediately volatilized and swept into the reaction zone of the furnace by a flow of argon with 10% hydrogen. The MWNTs grow perpendicularly from the surface of the quartz reactor tube. After the reaction, the pre-heater and the furnace were allowed to cool to room temperature in flowing argon, and the MWNT sheets collected. Precise details of the fabrication process are described in [25].

The resulting MWNTs were characterized by field-emission scanning electron microscopy. These studies confirm the collected material consists of highly aligned MWNTs with the dominant tube diameter in the range 20-25 nm with length 50 µm. The MWNT clumps were placed in toluene and then sonicated for 30 minutes to disperse the individual nanotubes, rinsed with isopropanol, and then allowed to dry. The nanotubes were then dispersed in a liquid SiO_2 solution (20 wt% SiO_2 nanoparticles dispersed in water, from [20]) such that a nanotube to SiO_2 dry-weight balance of 2:3 was obtained. The resulting solution was pipetted onto the inter-digital capacitor of the sensor.

Sensor Fabrication

A 2-cm square sensor was fabricated by photolithographically patterning a square spiral inductor and an interdigital capacitor on a Printed Circuit Board (PCB), see Fig. 1. An ≈150 µm thick layer of SiO_2 (confirmed by SEM imaging) followed by an ≈200 µm thick layer the MWNT-SiO_2 mixture were then coated onto the capacitor of the sensor, with a resulting sensor cross section as shown schematically in Fig. 4.

Experimental Setup for Sensing CO_2

The testing facility is schematically depicted in Fig. 2. The sensor was placed inside a sealed Plexiglas test chamber, and monitored with a single-turn 16 cm diameter loop-antenna located approximately 15 cm from the sensor. Test gas concentration was controlled with a mass flow controller (MKS Instruments Multi Gas Controller 647B).

The antenna impedance was measured with an impedance analyzer (Hewlett Packard 4396B), with the cable length removed from the measurement using an HP85033D calibration kit. A computer was used to control the mass flow controller and the impedance analyzer via a GPIB interface, as well as analyzing and processing the measurements.

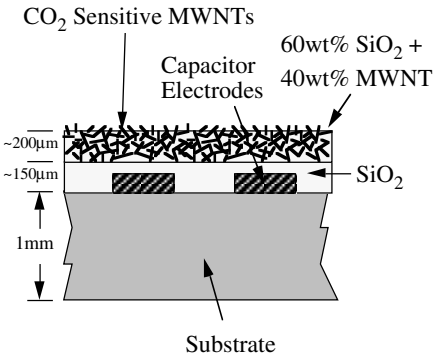

Fig. 4. Cross sectional view of the interdigital capacitor. An electrically insulating 150 µm-thick SiO_2 layer is first applied to protect the sensor, followed by a 200 µm MWNT-SiO_2 gas-sensing layer.

Results & Discussion

CO_2 Detection

Fig. 5 shows the response of the CO_2 sensor as it is alternately cycled between dry air (~80% N_2 and 20% O_2) and pure CO_2; the humidity level in the chamber was 0% RH, and the temperature was 23˚C. There is an increase in values of ε_r' and ε_r'', 0.040 (0.91%) and 0.035 (4.40%), respectively, as the gas is switched from CO_2 to dry air. The change in the complex permittivity magnitude $|\varepsilon_r|$ is 1.02%. The change in the complex permittivity is reversible, with no hysteresis observed.

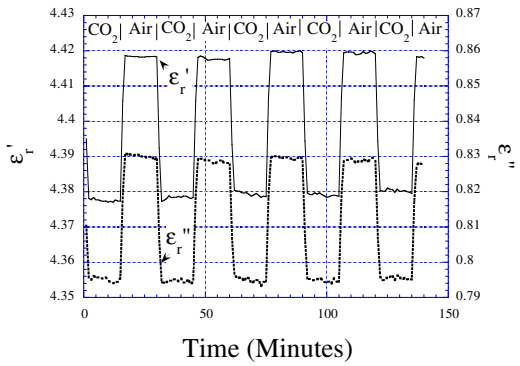

Fig. 5. Measured ε_r' and ε_r'' values when the sensor is cycled between pure CO_2 and dry air.

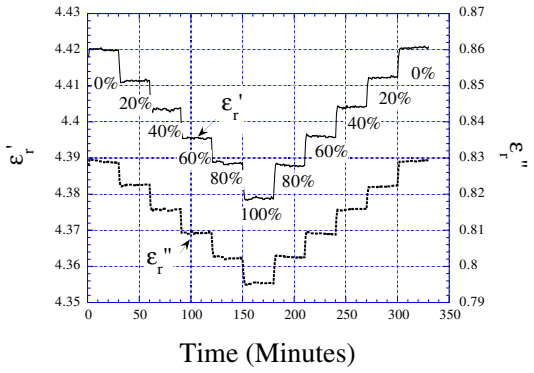

Fig. 6. Measured ε_r' and ε_r'' values when the sensor is exposed to CO_2 concentrations varying from 0% (volume) to 100% and then back to 0%. The shifts are linear, with $\Delta\varepsilon_r' = -0.0004043/\%CO_2$ and $\Delta\varepsilon_r'' = -0.0003476/\%CO_2$.

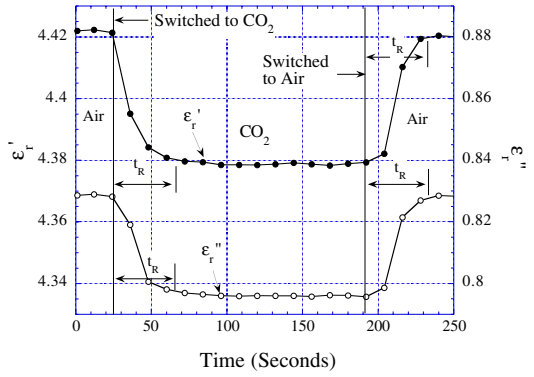

Fig. 7. Change in ε_r' and ε_r'' when the gas is switched from air to CO_2, and then back to air. The response time t_R, can be determined from the figure as less than 45 s.

As seen in Fig. 5 both ε_r' and ε_r'' of the MWNTs are lower when the sensor is exposed to CO_2 and higher when the sensor is exposed to dry air containing ~80 %N_2 and 20 % O_2. We believe that the change in ε_r'', which is directly proportional to the conductivity $\sigma = 2\pi f\ \varepsilon_0\varepsilon_r''$, is due to the adsorption and/or the insertion of gas molecules into either the core or surface of the MWNT that introduces defects and lowers the electrical conductivity [26]. As CO_2, N_2, and O_2 have a relative low ε_r' value (~1) compared to the MWNT graphene layer (ε_r'~15), the effective ε_r' of the exposed MWNT layer decreases as more gas molecules are adsorbed. Since CO_2 has two lone pair of electrons with Π-type C=0 bindings [27] and N_2 is an inert diatomic molecule that only reacts to graphene at high temperature [28], the adsorption capacity of CO_2 is much higher than N_2 at room temperature. Hence, there is a decrease in ε_r' and ε_r'' when the sensor is exposed to CO_2. While O_2, which has two lone-pair of electrons in the anti-

bonding Π orbital [29], has similar adsorption behavior as CO_2 it is not present in sufficient quantity to completely counter the N_2 effect. Our observations on ε_r'' (conductivity) decreasing with gas adsorption are consistent with those reported elsewhere [26,28,30,31].

Fig. 6 presents the shifts of ε_r' and ε_r'' as a function of the CO_2 to dry air volume ratio. The symmetry of the steps indicates the absence of hysteresis with increasing or decreasing CO_2 concentrations. The absolute change in the complex permittivity with CO_2 concentration is linear at $\Delta\varepsilon_r' = -0.0004043/\%CO_2$ and $\Delta\varepsilon_r'' = -0.0003476/\%CO_2$. The response time of the sensor t_R, determined as the time to achieve steady state response after switching gas concentrations, is determined from Fig. 7 as approximately 45 s, and was found to be constant with temperature to 43°C, the upper limit tested.

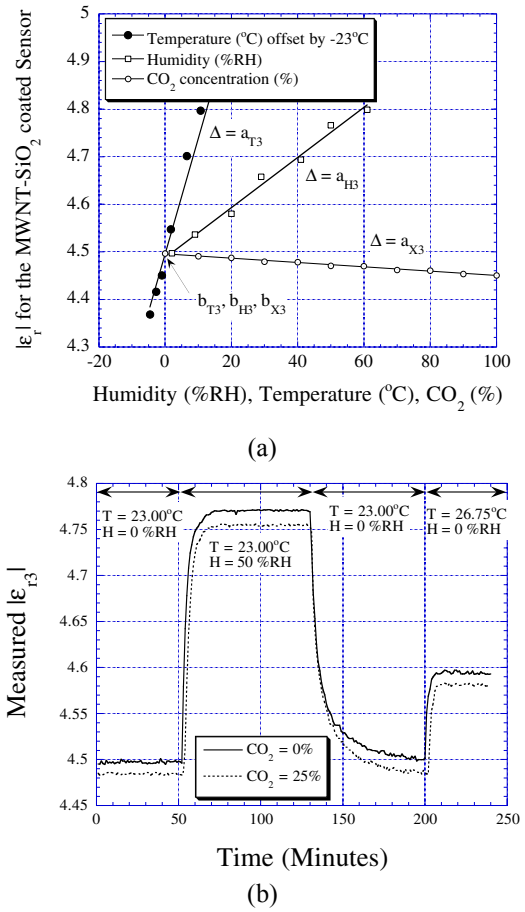

Fig. 8 (a) The permittivity magnitude of the MWNT-based CO_2 sensor shifts linearly with CO_2, humidity, and temperature. (b) The permittivity magnitude of the MWNT-based CO_2 sensor, at zero and 25% CO_2 concentration, as it is exposed to different humidity and temperature conditions.

Humidity and Temperature Dependencies

Fig. 8a displays the effect of changing humidity, temperature, and CO_2 concentration on the complex permittivity magnitude of the MWNT-SiO_2 sensor coating. Fig. 8b is an illustrative real-time measurement showing how the permittivity magnitude of the MWNT CO_2 sensor changes, at CO_2 concentration = 0% and 25%, in response to various humidity and temperature conditions. Due to the strong attraction of the MWNTs for water moisture the response time of the CO_2 sensor suffers a dramatic increase in high humidity environments. Operation at elevated temperatures improves the response time of the sensor as it is cycled between dry and humid environments. Switching from 0% to 100% humidity levels at 23°C, 31°C, and 42°C the response times are, respectively, 22, 16 and 14 minutes. Switching from 100% to 0% humidity levels at 23°C, 31°C, and 42°C the response times are, respectively, 58, 36 and 34 minutes.

To eliminate the effects of humidity and temperature, a SiO_2-coated sensor and an uncoated sensor are used in addition to the CO_2 sensor, forming a sensor array. The SiO_2-coated and the plain sensors do not respond to CO_2, but both linearly respond in separable ways to humidity and temperature, over the range investigated 0 - 60% RH and 18˚C - 43˚C, as shown in Figs. 9a and 9b. Since their responses to both humidity and temperature are linear, the complex permittivity magnitude of the plain sensor ε_{r1}, and the SiO_2-coated sensor ε_{r2}, can be related to humidity and temperature as:

$$\varepsilon_{r1} = \left(a_{T1}T + b_{T1}/2\right) + \left(a_{H1}H + b_{H1}/2\right) \quad (4)$$

$$\varepsilon_{r2} = \left(a_{T2}T + b_{T2}/2\right) + \left(a_{H2}H + b_{H2}/2\right) \quad (5)$$

H is humidity in %RH, T is temperature in ˚C, while a and b are coefficients experimentally determined by curve-fitting the data in Figs. 8b-8c and listed in Table 1. In our experiment, T was offset by -23˚C (i.e. $T = 0$ means $T = 23$˚C in the real world); the offset is required since the sensor is initially calibrated at room temperature (23˚C). The humidity and temperature can then be determined by simultaneously solving Eqs. (4) and (5):

$$\begin{bmatrix} T \\ H \end{bmatrix} = \frac{1}{a_{T1}b_{H2} - a_{T2}b_{H1}} \begin{bmatrix} b_{H2} & -b_{H1} \\ -a_{T2} & a_{T1} \end{bmatrix} - \begin{bmatrix} \varepsilon_{r1} - (b_{T1} + b_{H1})/2 \\ \varepsilon_{r2} - (b_{T2} + b_{H2})/2 \end{bmatrix} \quad (6)$$

For the MWNT-SiO_2 coated sensor the magnitude of the complex permittivity ε_{r3} can be related to humidity, temperature, and CO_2 with the equation:

$$\varepsilon_{r3} = \left(a_{T3}T + b_{T3}/3\right) + \left(a_{H3}H + b_{H3}/3\right) + \left(a_{X3}X + b_{X3}/3\right) \quad (7)$$

X is the percent volume of CO_2 present, and a_{T3}, a_{H3}, a_{X3}, b_{T3}, b_{H3}, and b_{X3} are coefficients determined from Fig. 8a listed in Table 1. Rearranging Eq. (7), the CO_2 concentration can be found as:

$$X = \frac{\varepsilon_{r3} - a_{T3}T - a_{H3}H - \left(b_{T3} + b_{H3} + b_{X3}\right)/3}{a_{X3}} \quad (8)$$

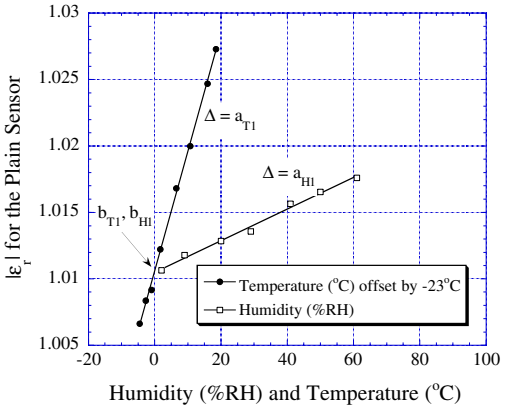

(a)

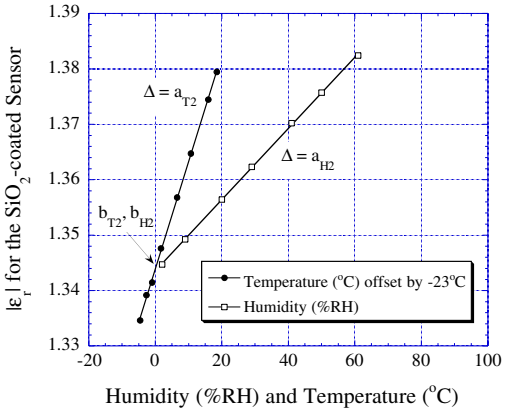

(b)

Fig. 9. (a) The permittivity magnitude of the plain (uncoated) sensor shifts linearly with humidity or temperature. (b) The permittivity magnitude of the SiO_2-coated sensor shifts linearly with humidity or temperature; note response slopes of Figs. 8a, 9a, and 9b are uniquely different.

Fig. 10 shows application of the sensor array to measurement of 0% and 25% CO_2 atmospheres in a variable temperature and humidity environment; the CO_2 percentage is calculated using Eq. (8) with data from Fig. 8b. After a calibration transient due to the different response times of the sensors to changing temperature and humidity levels (primarily dictated by the strong attraction of MWNTs to water vapor), the calculated CO_2 levels in a given humidity and temperature environment are within an error margin of ± 3 CO_2%. However since the periods over which the sensor reports spurious measurement values are clearly discernable, both due to the rapid rate of change and clearly incorrect values (e.g. 120% CO_2), software routines could be readily implemented to keep the sensor tracking nominal steady-state values.

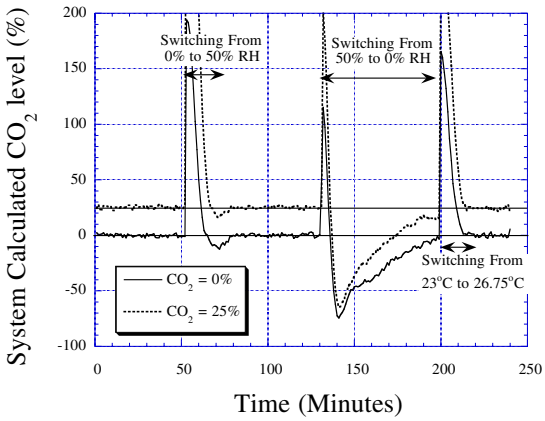

Fig. 10. CO_2 concentration determined using measured data as corrected by Eq. 8 with calibration parameters of Table 1; measurements are taken with CO_2 concentration kept at 0% and 25%. Outside of the transient region, upon reaching steady state measured results are within ± 3%. Since the different sensors have different response rates large errors occur when humidity and temperature change, an effect dominated by the slow desorption of moisture from the MWNTs.

Conclusions

Application of multi-wall carbon nanotubes (MWNTs) to CO_2 sensing has been demonstrated. The sensor is reversible, with no hysteresis observed between the cycles of CO_2 and dry air (~20% O_2 + 80% N_2), with a response time of approximately 45 s. The MWNTs are used in combination with a passive, remote query sensor platform, therefore no direct wire connections to the sensor are needed for operation, nor is a battery needed to power the sensor. These operational characteristics make the CO_2 sensor attractive for long-term wireless monitoring applications, such as monitoring CO_2 levels in food or medicine packages to check for product spoilage [12,13].

It is found that the complex permittivity of the MWNTs is lower when the sensor is exposed to CO_2 than in dry air. This is due to the relatively higher adsorption capacity of the MWNT for CO_2 in comparison to N_2, which increases

the surface defects [26] and lowers the MWNT conductivity. Our observations on ε_r'' (conductivity) decreasing with gas adsorption are consistent with those reported elsewhere [26,28,30,31]. Absorption of CO_2 also lowers ε_r' of the MWNT, as ε_r' of CO_2 is much smaller than that of the electrically conductive MWNT. While O_2, which has two lone-pair of electrons in the anti-bonding Π orbital [29], has similar adsorption behavior as CO_2 it is not present in sufficient quantity to completely counter the N_2 effect.

To eliminate the deleterious effects of humidity and temperature on the MWNT CO_2 sensor, measured values are calibrated against the response of both a SiO_2-coated sensor, and a plain (uncoated) sensor, neither of which response to CO_2 and both of which uniquely respond to temperature and humidity. Using the described calibration algorithm of Eq. 8 enables CO_2 concentrations to be measured to within ±3 CO_2% in a changing humidity and temperature environment. For operation within 0 - 60% RH and 18˚C - 43˚C the sensors respond linearly to humidity and temperature, therefore a straight-forward linear calibration routine can be used with success. At higher temperatures and humidity levels the sensor responses are non-linear, so a higher-order calibration routine would be needed to maintain sensor accuracy.

Table 1: Regression coefficients of plain, SiO_2 coated, and MWNT-SiO_2 coated sensors.

Coefficients	Plain Sensor	SiO_2-coated Sensor	MWNT-coated Sensor
a_T	$a_{T1} = 0.00089523$	$a_{T2} = 0.00193071$	$a_{T3} = 0.024175$
b_T	$b_{T1} = 1.01062$	$b_{T2} = 1.34392$	$b_{T3} = 4.49524$
a_H	$a_{H1} = 0.00011883$	$a_{H2} = 0.00064168$	$a_{H3} = 0.0052665$
b_H	$b_{H1} = 1.01051$	$b_{H2} = 1.34359$	$b_{H3} = 4.49472$
a_X	0	0	$a_{X3} = -0.00045769$
b_X	0	0	$b_{X3} = 4.49562$

References

[1] de Heer W A, Chatelain A, and Ugarte D. A carbon nanotube field-emission electron source. Science 1995;270:1179.

[2] Tans S, Verschueren A, Dekker C. Room-temperature transistor based on a single carbon nanotube. Nature 1998;393:49.

[3] Martel R, Schmidt T, Shea H R, Hertel T, Avouris Ph. Single- and multi-wall carbon nanotubes field-effect transistor. Appl. Phys. Lett. 1998;73:2447.

[4] Tan S, Devoret M, Dai H Thess A, Smalley R, Geerligs L, Dekker C. Individual single-wall carbon nanotubes as quantum wires. Nature 1997;386:474.

[5] Yao Z, Postma H, Balents L, Dekker C. Carbon nanotube intramolecular junctions. Nature 1999;402:273.

[6] Baughman R H, Cui C, Zakhidov, Iqbal Z, Barasci J N, Spinks G M, Wallace G G, Mazzoldi A, Rossi D de, Rinzler A G, Jaschinski O, Roth S, Kertesz M. Carbon Nanotube Actuators. Science 1999;284:1340-1342.

[7] Rueckes T, Kim K, Joselevich E, Tseng G Y, Cheung C, Lieber C M. Carbon Nanotube-Based Nonvolatile Random Access Memory for Molecular Computing. Science 2000;289:94-97.

[8] Kong J, Franklin N R, Zhou C, Chapline M G, Peng S, Cho K, Dai H. Nanotube Molecular Wires as Chemical Sensors. Science 2000;287:622-625.

[9] Bienfait M, Asmussen B, Johnson M, Zeppenfeld P. Methane mobility in carbon nanotubes. Surface Science 2000;460:243.

[10] Ong K G, Grimes C A. A Resonant Printed-circuit Sensor for Remote Query Monitoring of Environmental Parameters. Smart Mater. Struct. 2000;9:421-428.

[11] Ong K G. Design And Application Of Planar Inductor-Capacitor Resonant Circuit Remote Query Sensors, University of Kentucky Dissertation, August 2000. Available upon request from corresponding author, or through University Microfilms, Ann Arbor MI.

[12] Sheppard N, Tucker R, and Salehi-Had S. Design of a conductimetric pH microsensor based on reversibly swelling hydrogels. Sensors and Actuators B 1993;10:73-77.

[13] Dalgaard P, Mejlholm O, Huss H H. Application of an interactive approach for development of a microbial model predicting the shelf-life of packed fish. Int. J of Food Microbiology 1997;38:69-179.

[14] Well S L and DeSimone J. CO_2 Technology Platform: An Important Tool for Environmental Problem Solving. Angew. Chem. Int. Ed. 2001;40:518-527.

[15] Lindgren T, Norback D, Anderson K, Dammstrom B. Cabin environment and perception of cabin air quality among commercial aircrew. Aviation, Space, and Environmental Medicine 2000;71(8):774-482.
[16] Endres H-E, Hartinger R, Schwaiger M, Gmelch G, Roth M. A Capacitive CO_2 Sensor System with Suppression of the Humidity Interference. Sensors and Actuators B 1999;57:83-87.
[17] Lee M S, Meyer J U. A New Process for Fabricating CO_2-Sensoing Layers Based on $BaTiO_3$ and Additives. Sensors and Actuators B 2000;68:293-299.
[18] Matsubara S, Kaneko S, Morimoto S, Shimizu S, Ishihara T, Takita Y. A Practical Capacitive Type CO_2 Sensor Using $CeO_2/BaCO_3/CuO$ Ceramics. Sensors and Actuators B 2000;65:128-132.
[19] Currie J F, Essalik A, Marusic J C. Micromachined Thin Film Solid State Electrochemical CO_2, NO_2, and SO_2 Gas Sensors. Sensors and Actuators B 1999;59:235-241.
[20] Chemat Technology, Inc. 9036 Winaetka Ave., Northridge, CA. http://www.chemat.com.
[21] Ramo S, Whinnery J R, Van Duzer T. Fields and Waves in Communication Electronics, John Wiley & Sons, Inc, Chap. 13, 1984.
[22] Brian H E. Printed Inductors and Capacitors. Tele-Tech & Electronic Industries 1954;14:68-69.
[23] Markx G H and Davey C L. The Dielectric Properties of Biological Cells at Radiofrequencies: Applications in Biotechnology. Enzyme and Microbial Technology 1999;25:161-171.
[24] Endres H E, Drost S. Optimization of the geometry of gas-sensitive interdigital capacitor. Sensors and Actuators B 1991;4:95-98.
[25] Andrews R, Jacques D, Rao A M, Derbyshire F, Qian Q, Fan F, Dickey E C, and Chen J. Continuous Production of Aligned Carbon Nanotubes: A step Closer to Commercial realization. Chem. Phys. Lett. 1999;303:467-474.
[26] Marliere C, Poncharal P, Vaccarini L, Zahab A. Effect of gas adsorption on the electrical properties of single-walled carbon nanotubes mats. Materials Research Soc. Sym. Proc. 2000;539:173-178.
[27] Walker Jr P L. Chemistry and Physics of Carbon. Marcel Dekker, Inc., New York, 6, 1970.
[28] Sumanasekera G U, Adu C K W, Fang S and Eklund P C. Effects of gas adsorption and collisions on electrical transport in single walled carbon nanotubes. Phy. Rev. Lett. 2000;85:1096-1099.
[29] Kleinberg J, Argersinger Jr W J, and Griswold E. Inorganic Chemistry. D.C. Health and Co., Boston, 1960.
[30] Stepanek I, de Menorval L C, Edwards R, Bernier P. Carbon nanotubes and gas adsorption. AIP Conference Proc. 1999;486:456-461.
[31] Collins P G, Bradley P G, Ishigami K, and Zettl A. Extreme Oxygen Sensitivity of Electronic Properties of Carbon Nanotubes. Science 2000;287:1801-1804.

Acknowledgements

This work was supported by the National Science Foundation under grant numbers DMR-9809686 and ECS-9875104.